Journal of Advanced Marine Engineering and Technology, Vol. 45, No. 3, pp. 88~93, 2021
J. Advanced Marine Engineering and Technology (JAMET)
https://doi.org/10.5916/jamet.2021.45.3.88

ISSN 2234-7925 (Print)
ISSN 2765-4796 (Online)
Original Paper

Effect of analyzer scan time on the oxygen storage capacity performance in Pd-based TWCs

Daekun Kim†

(Received March 19, 2021 ; Revised April 14, 2021 ; Accepted May 12, 2021)

Abstract: Oxygen storage materials play an important role in increasing the performance of three-way catalysts. However, high operating temperatures and lubricant additives result in a reduction in the oxygen storage capacity (OSC), thus shortening the life of the catalyst. Therefore, it is important to measure and investigate OSCs using an appropriate protocol to evaluate catalyst's performance and deactivation. In this study, the effect of analyzer scan time on the OSC performance of a commercial monolith three-way catalyst containing oxygen storage materials such as cerium-zirconium mixed oxide was investigated in a bench-flow reactor, and an appropriate scan time was suggested based on these results. This study also investigated OSC as a function of inlet gas temperatures between 300 and 550 °C. The results suggest that the OSC experiment should be performed using a scan time of at least 4.0 s, while reliable dynamic OSC results cannot be obtained if the analyzer scan time is longer than 4 s. Therefore, a study is required in order to determine the optimal OSC scan time to ensure accuracy, while also retaining an acceptable level of resolution. It was also confirmed that the OSC increases with increasing inlet gas temperature up to a temperature of 450 °C, but no longer increases above 450 °C.

Keywords: Pd-based three-way catalyst, Oxygen storage capacity, Ceria-zirconia mixed oxide, Bench-flow reactor

1. Introduction

Three-way catalysts (TWCs) are widely used to effectively control the emission of nitrogen oxides (NOx), carbon monoxide (CO), and hydrocarbons (HCs), which are harmful substances contained in the exhaust gases of gasoline engines, by converting them into nitrogen (N_2), carbon dioxide (CO_2), and water vapor (H_2O) **[1]**. The three-way catalytic conversion efficiencies of NO, CO, and unburnt hydrocarbons (UHCs) exhibited the highest performance at air-fuel (A/F) ratios close to the stoichiometric point (14.7: 1). However, under excessive air supply conditions (fuel-lean conditions above A/F = 14.7, or $\lambda = 1$), the reaction of NO reductants with excessive air causes a shortage of the NO reducing agent, which significantly reduces NO conversion. Therefore, gasoline engines are designed to operate in narrow bands or windows close to the stoichiometric ratio, and an oxygen (O_2) sensor (or lambda sensor) must be installed downstream of the catalytic converter to determine the optimal A/F ratio for the conversion of harmful gases. However, engine operating conditions which change frequently during operation can induce A/F ratio oscillations owing to the feedback from the O_2 sensor to the engine control unit, making it difficult to maintain stoichiometric points. For this reason, cerium oxide (CeO_2), a well-known oxygen storage material, is added to the washcoat to improve the conversion efficiency of CO, HC, and NOx by storing and releasing O_2 according to Ce^{4+}/Ce^{3+} redox reactions **[2][3]**. However, pure CeO_2 generally exhibits poor thermal stability and weak metal-CeO_2 interactions **[4]-[6]**. To enhance the thermal stability of TWCs, several other oxides such as zirconia (ZrO_2), silicon dioxide (SiO_2), barium oxide (BaO), and lanthanum oxide (La_2O_3) have been added to the catalyst in appropriate quantities **[7]-[17]**.

In accordance with the recently revised United States Environmental Protection Agency standard Tier 3 regulations, catalyst lifespan regulations have been strengthened from 12,000 miles to 150,000 miles. To meet this requirement, ongoing efforts have been made to determine the causes of catalyst deactivation, thereby extending the catalyst life. One general cause of catalyst deactivation is the degradation of the oxygen storage capacity (OSC) due to high temperature exposure, which may occur as a result of the agglomeration of the oxygen storage material, or a reduction in catalytic activity owing to the contact between the sintered precious metal and oxide support **[18]-[20]**. In addition, deactivation of TWC performance has been attributed to the formation of cerium orthophosphate ($CePO_4$) and zinc pyrophosphate ($Zn_2P_2O_7$) compounds within the washcoat of the catalyst caused by lubricant additives (poisoning) **[21]-[26]**.

† Corresponding Author (ORCID: https://orcid.org/0000-0003-2662-6741): Researcher, Department of Mechanical Engineering, University of Tennessee, 1512 Middle Drive, Knoxville, TN, 37996, USA, E-mail: kkun@vols.utk.edu, Tel: +01-865-347-7226

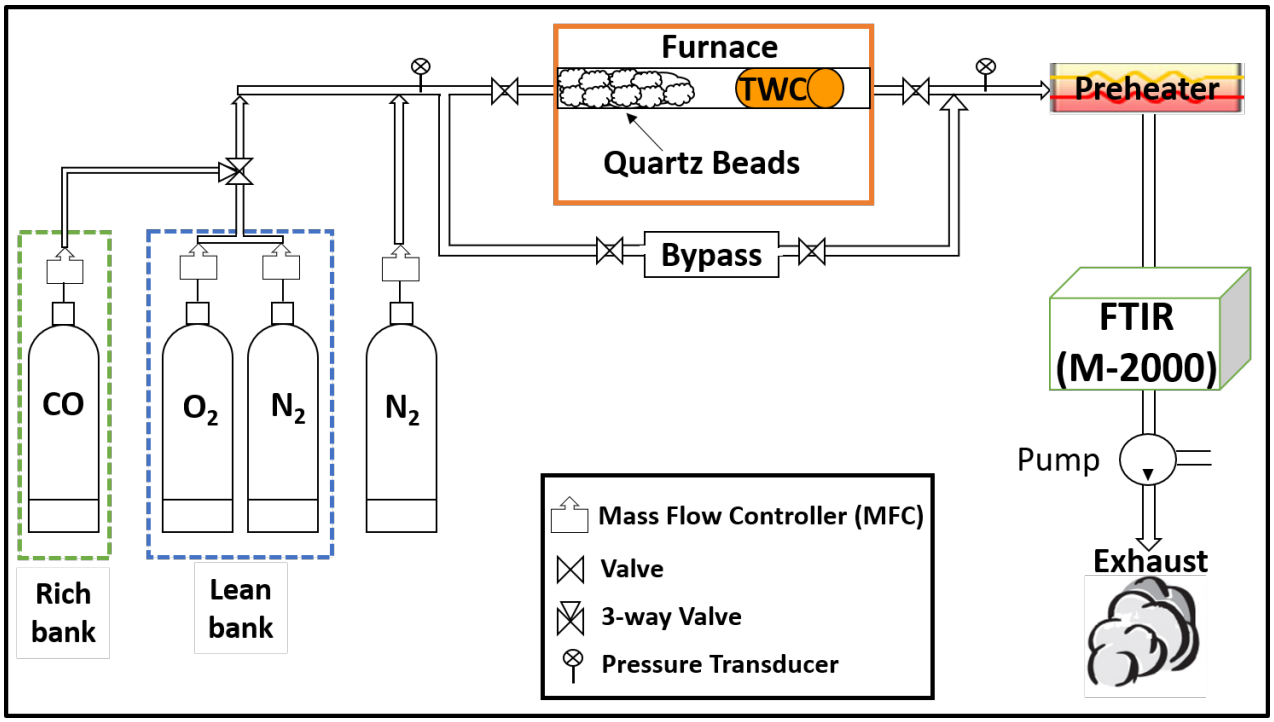

Figure 1: Schematic diagram of the bench flow reactor (BFR) system. More details can be found in **[26][27]**.

The OSC experiment is one of the several studies that has investigated the performance and deactivation of TWC by probing the performance of CeO_2, an oxygen storage material and a key component of the TWC washcoat. However, protocols for obtaining accurate results from OSC experiments performed in a bench flow reactor (BFR) using a Fourier transform infrared (FTIR) analyzer and explanations of the effects of these experimental procedures on the OSC results are lacking. Herein, this study presents an experimental method for dynamic OSC measurement in a BFR, while the effect of the scan time of FTIR on OSC results was investigated using a Pd-based TWC.

2. Experimental Apparatus and Procedure

2.1 Bench flow reactor system

Figure 1 shows a schematic of the BFR system. The BFR mainly consists of mass flow controllers (MFCs), a quartz tube reactor enclosed in a temperature-programmable furnace, and an FTIR spectrometer. A more detailed explanation of the BFR is provided in a previous study **[26][27]**. For this experiment, a three-way switching valve was installed in the BFR to alternate the flow between the lean and rich banks. Each gas that passed through the MFCs was supplied from an individual gas cylinder. The CO and CO_2 concentrations at the inlet and exit were measured with an MIDAC-M2000 FTIR spectrometer using the software Essential FTIR.

2.2. Three-way catalyst

The TWCs used for OSC measurements in the present study were obtained from a 2009 MY Jeep Liberty V6 from a local dealership. Inductively coupled plasma mass spectrometry (ICP-MS), electron probe microanalysis (EPMA), and X-ray diffraction (XRD) analyses were used to identify cerium (Ce), the oxygen storage material in the catalyst, as follows. ICP-MS analysis confirmed that this Pd-based TWC was primarily composed of Mg, Al, Ba, Ce, and Zr. In addition, precious metals, palladium (Pd) and rhodium (Rh), were detected in a weight ratio of 8:1 with respect to the bulk material. In a previous paper **[26]**, the peak of mixed oxides ($Ce_xZr_{1-x}O_2$) was clearly detected in the XRD pattern at $2\theta = 29.2°$.

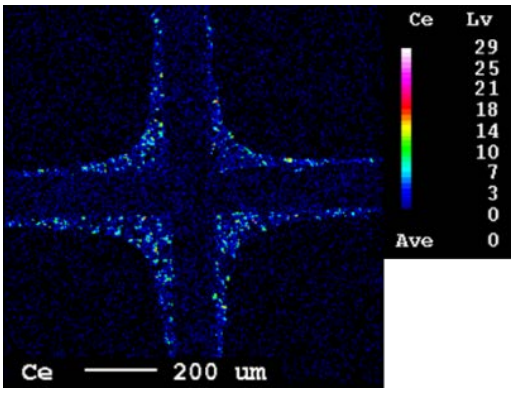

Figure 2: EPMA element map of cerium (Ce) in the TWC sample

Figure 2 shows the EPMA element map of Ce for the Pd-based TWC sample. As shown in **Figure 2**, the results obtained from the EPMA elemental map confirm the presence of Ce in the washcoat of the TWC. Although Ce could not be detected quantitatively, it was confirmed that the OSC material of the Pd-based TWC was Ce-Zr mixed oxides.

2.3 Oxygen storage capacity evaluation protocol

Although FTIR spectroscopy cannot measure homonuclear diatomic molecules such as N_2 and O_2, it is a suitable analyzer for OSC investigations as multiple gaseous species, such as CO and CO_2, can be measured simultaneously and in real time at high temperatures. The O_2 storage reaction under lean conditions and OSC reduction reaction under rich conditions are given by the following reactions **[28]**:

$$Ce_2O_3 + 0.5O_2 \leftrightarrow 2CeO_2 \quad (1)$$

$$CO + 2CeO_2 \leftrightarrow Ce_2O_3 + CO_2 \quad (2)$$

Figure 3 shows the CO and CO_2 data plotted as a function of time to quantify the OSC. During the lean cycle, O_2 is stored in the cerium (**Equation 1**), and the stored O_2 is subsequently released and reacts with CO during the rich cycle to produce CO_2 (**Equation 2**). The OSC was calculated as a normalized value as a function of the volume for the TWC (g-O_2/L-catalyst) through an integration of the quantity of CO_2 produced under rich conditions.

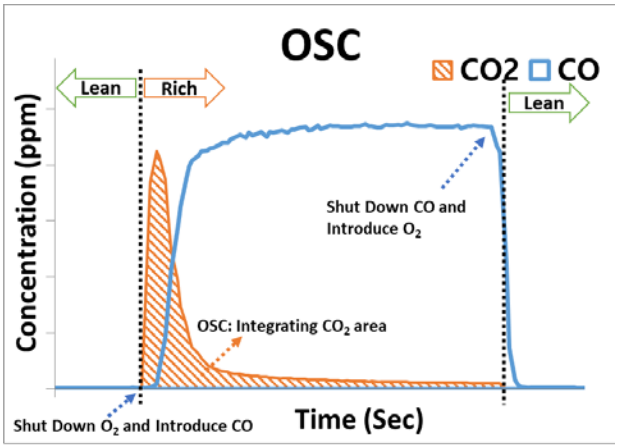

Figure 3: Example of CO and CO_2 curves for OSC measurement

Prior to a performance evaluation of the BFR, the fresh TWC sample was subjected to a degreening process in order to enhance its stability. The gas composition during the degreening process consisted of 10% CO_2, 10% H_2O, and 80% N_2 supplied at a gas hourly space velocity (GHSV) of 60,000 h^{-1} and a gas inlet temperature of 700°C for four h.

Table 1: Gas compositions for OSC

Mode	Time	Gas Composition
Lean	120 s	0.73% O_2, balance N_2
Rich	120 s	0.50% CO, balance N_2

An OSC experiment was carried out for the fresh TWC sample under a slow cycle consisting of 120 s lean and 120 s rich for a total of four cycles (total duration of 720 s) in a temperature range between 300 and 550°C measured in 50°C increments at a GSHV of 60,000 h^{-1}. The feed gas compositions during the lean and rich cycles are listed in **Table 1**. N_2 gas was introduced at each temperature for approximately 10 min prior to the OSC measurement to remove any residual CO from the precious metal sites still present from the last cycle at the previous temperature. To investigate the effect of the FTIR scan time on the OSC results, the OSC experiment on the fresh sample was performed at two different FTIR scan times (1.5 s and 9.0 s) by varying the spectral resolution.

3. Results and Discussion

Figures 4 (a) and (b) show the results of the oxygen storage process during the lean/rich cycle at an inlet gas temperature of 350 °C using FTIR scan times of 9.0 s (shown in 4a) and 1.5 s (shown in 4b). As described in section 2.3, O_2 is stored in a mixed oxide on Pd sites during the lean cycle and subsequently released during the rich cycle. The O_2 released during this process reacts with CO during the rich cycle to produce CO_2, as shown in **Figure 4**.

Since the OSC is calculated as an average value using the CO_2 produced under rich conditions, it is necessary to ensure that the amount of CO_2 produced is similar in each cycle for obtaining accurate OSC measurements. As shown in **Figure 4 (a)**, when a scan time of 9.0 s was used, the CO concentration remained constant during the rich cycle, while the concentration of CO_2 produced varied with each cycle. In contrast, when a scan time of 1.5 s was used, the CO concentration remained constant throughout all rich cycles, while the amount of CO_2 produced also remained constant, as shown in **Figure 4 (b)**. These results indicate that OSC measurements should be performed before reaching the maximum CO_2 production and that a scan time of 9.0 s is insufficient. In essence, OSC measurements obtained from a

scan time of 9.0 s yield inaccurate results exhibiting large deviations. A detailed explanation is provided below and is illustrated in **Figure 5**. Also noteworthy is the point at which the CO_2 concentration increased as the local environment transitioned from rich to lean conditions. For example, between 240 s and 250 s, the CO_2 concentration increased to a local maximum and then rapidly decreased. This occurred as a result of the CO being retained in the line during the switch from rich to lean conditions being fed to the catalyst along with the supplied O_2 using the 3-way valve. Therefore, this period of overlap should be excluded from the OSC calculations.

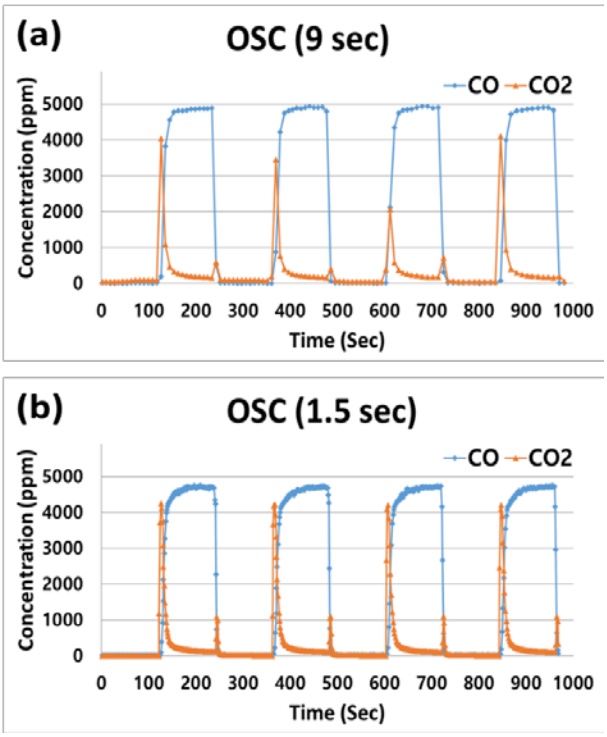

Figure 4: Full scale OSC with resulting CO and CO_2 concentration for the fresh sample obtained from FTIR scan times of (a) 9.0 s and (b) 1.5 s at an inlet gas temperature of 350°C

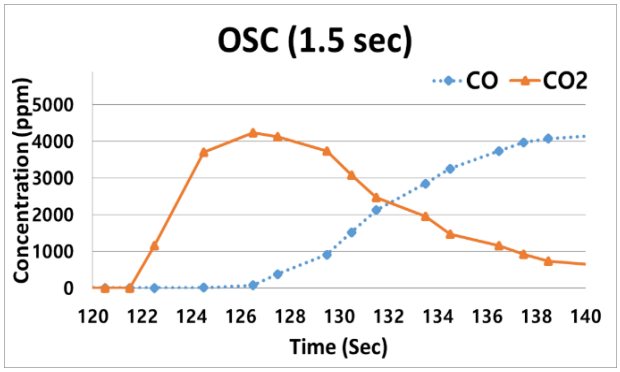

Figure 5: An expanded portion of **Figure 4 (b)** between 120 s and 140 s

Table 2: OSC results of the fresh sample at two different FTIR scan times

Scan time	OSC [in g-O_2/L-catalyst]				
	1st	2nd	3rd	4th	Average ± σ
1.5 s	0.728	0.715	0.709	0.713	0.716 ± 0.008
9.0 s	0.822	0.716	0.536	0.925	0.750 ± 0.166

Based on the CO_2 curve generated in **Figure 4**, OSCs for 1.5 and 9.0 s scan times from each cycle were obtained and are listed in **Table 2**, including the standard deviation (σ). As expected, the OSC deviation obtained from a 1.5 s scan time is significantly lower than that with a 9.0 s scan time.

The magnified section of **Figure 4** at a time between 120 and 140 s is shown in **Figure 5** and indicates a suitable FTIR scan time for OSC measurements. A significant increase in the CO_2 concentration was observed owing to the reaction of the stored O_2 with the CO introduced between 120.0 s and 124.5 s, with the CO_2 concentration decreasing after 124.5 s. Therefore, at an inlet gas temperature of 350 °C, it can be determined that the OSC should be obtained in less than 4 s. This is the amount of time required to perform the FTIR scan prior to reaching the point of maximum CO_2 formation.

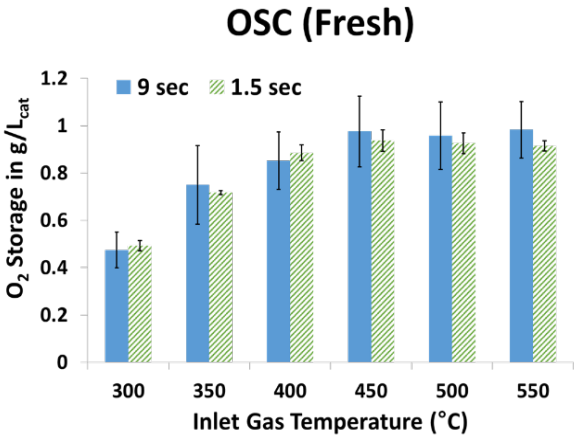

Figure 6: OSC comparison with different FTIR scan times at temperatures between 300 and 550°C

Figure 6 shows a comparison of the OSC results obtained from two different FTIR scan times in the temperature range between 300–550°C measured in 50°C increments. As **Figure 6** shows, the inlet gas temperature has a significant effect on the OSC. It has been observed in previous studies that OSC performance is strongly dependent on temperature **[18][29]**. The OSC results obtained from the 1.5 s and 9.0 s FTIR scan times show that the higher the inlet gas temperature, the higher the OSC. However,

when the inlet gas temperature exceeded 450°C, the OSC no longer continued to increase for either FTIR scan time. In a previous study **[30]**, it was observed that the OSC no longer increases at temperatures above 450°C owing to oxygen storage limitations as a result of bulk diffusion. However, the OSC obtained from a 9.0 s FTIR scan time exhibited a larger standard deviation than the OSC obtained from a 1.5 s FTIR scan time. At a 1.5 s FTIR scan time, the OSC results obtained were repeatable across all temperature ranges.

4. Conclusions and Recommendations

In the present investigation, the effect of FTIR scan times on the OSC results of Pd-based TWCs were investigated. OSC materials such as Ce and Zr present in TWCs were identified qualitatively through surface characterization techniques such as XRD, EPMA, and ICP-MS analysis. In addition, the OSC performance was evaluated over feed gas temperatures ranging between 300 and 550°C measured in 50°C increments. This study revealed the following points regarding the effect of the FTIR scan time and inlet gas temperature on the OSC results.

1) With a 9.0 s FTIR scan time, the OSC results are unreliable due to the significant variations in CO_2 production during each rich cycle period.
2) Measuring the OSC with a short FTIR scan time (1.5 s) obtained reliable OSC results exhibiting similar CO_2 production curves for each rich cycle period.
3) These results indicate that in order to reduce the experimental error of the OSC results, it is necessary to determine a suitable FTIR scan time that can be used to evaluate the OSC performance of the TWC in the BFR using an FTIR analyzer. As far as the FTIR performance permits, it is advisable to measure the OSC using rapid scan times, but if not, it is recommended to measure the OSC using an FTIR scan time of at least 4 s to obtain reliable results. (See **Figure 5**).
4) When calculating the OSC, the CO_2 produced in the process of switching the 3-way valve from rich to lean should be excluded.
5) For the Pd-based TWC used in this study, the OSC increased with increasing temperature up to 450°C. Above 450°C, no further increase in the OSC occurred.

The most significant finding in this investigation was that shorter FTIR scan times yield more reliable OSC results. However, short FTIR scan times can only be obtained by reducing the FTIR resolution. Therefore, before performing OSC experiments using FTIR, a further investigation should be conducted to determine the optimal scan time to obtain accurate dynamic OSC results.

Author Contributions

Conceptualization, D. K. Kim; Methodology, D. K. Kim; Validation, D. K. Kim; Experiments, D. K. Kim; Resources, D. K. Kim; Data Curation, D. K. Kim; Results Analysis, D. K. Kim; Writing-Original Draft Preparation, D. K. Kim; Writing-Review & Editing, D. K. Kim; Visualization, D. K. Kim; Supervision, D. K. Kim.

References

[1] M. V. Twigg, “Progress and future challenges in controlling automotive exhaust gas emissions,” Applied Catalysis B Environmental, vol. 70, no. 1-4, pp. 2-15, 2007.

[2] J. Wang, H. Chen, Z. Hu, M. Yao, and Y. Li, “A review on the Pd-based three-way catalyst,” Catalysis Reviews - Science and Engineering, vol. 57, no. 1, pp. 79-144, 2015.

[3] H. S. Gandhi, *et. al*, “Laboratory evaluation of three-way catalysts,” SAE Transactions, pp. 901-912, 1976.

[4] J. Kašpar, P. Fornasiero, and N. Hickey, “Automotive catalytic converters: current status and some perspectives,” Catalysis today, vol. 77, no. 4, pp. 419-449, 2003.

[5] J. Kašpar, P. Fornasiero, and M. Graziani, “Use of CeO_2-based oxides in the three-way catalysis,” Catalysis Today, vol. 50, no. 2, pp. 285-298, 1999.

[6] M. Shelef, G. W. Graham, and R. W. McCabe, “Ceria and other oxygen storage components in automotive catalysts,” Catalysis by Ceria and related Materials, pp. 343-375, 2002.

[7] M. Ozawa and M. Kimura, “Effect of cerium addition on the thermal stability of gamma alumina support,” Journal of Materials Science Letters, vol. 9, pp. 291-293, 1990.

[8] P. Burtin, J. P. Brunelle, M. Pijolat, and M. Soustelle, “Influence of surface area and additives on the thermal stability of transition alumina catalyst supports. I: Kinetic data,” Applied Catalysis, vol. 34, pp. 225-238, 1987.

[9] B. Beguin, E. Garbowski, and M. Primet, “Stabilization of alumina toward thermal sintering by silicon addition,” Journal of Catalysis, vol. 127, no. 2, pp. 595-604, 1991.

[10] T. Yamamoto, T. Hatsui, T. Matsuyama, T. Tanaka, and T. Funabiki, “Structures and acid-base properties of La/Al_2O_3-

role of La addition to enhance thermal stability of γ-Al_2O_3," Chemistry of Materials, vol. 15, no. 25, pp. 4830-4840, 2003.

[11] J. H. Kwak, J. Hu, A. Lukaski, D. H. Kim, J. Szanyi, and C. H. F. Peden, "Role of pentacoordinated Al_3^+ ions in the high temperature phase transformation of γ-Al_2O_3," The Journal of Physical Chemistry C, vol. 112, no. 25, pp. 9486-9492, 2008.

[12] H. S. Gandhi, G. W. Graham, and R. McCabe, "Automotive exhaust catalysis," Journal of Catalysis, vol. 216, no. 1-2, pp. 433-442, 2003.

[13] H. Muraki, H. Shinjoh, and Y. Fujitani, "Effect of lanthanum on the no reduction over palladium catalysts," Applied Catalysis, vol. 22, no. 2, pp. 325-335, 1986.

[14] G. B. Fisher, J. R. Theis, M. V Casarella, and S. T. Mahan, "The role of ceria in automotive exhaust catalysis and OBD-II catalyst monitoring," SAE Technical Paper, no. 931034, 1993.

[15] A. Kato, H. Yamashita, H. Kawagoshi, and S. Matsuda, "Preparation of larnthanum β-alumina with high surface area by coprecipitation," Journal of American Ceramic Society, vol. 70, no. 7, pp. C-157, 1987.

[16] I. I. M. Tijburg, J. W. Geus, and H. W. Zandbergen, "Application of lanthanum to pseudo-boehmite and γ-Al_2O_3," Journal of Materials Science, vol. 26, no. 23, pp. 6479-6486, 1991.

[17] M. Machida, K. Eguchi, and H. Arai, "Preparation and characterization of large surface area $BaO{\cdot}6Al_2O_3$," Bulletin of the Chemical Society of Japan, vol. 61, no. 10, pp. 3659-3665, 1988.

[18] H. C. Yao and Y. F. Y. Yao, "Ceria in automotive exhaust catalysts: I. Oxygen storage," Journal of Catalysis, vol. 86, no. 2, pp. 254-265, 1984.

[19] S. Bedrane, C. Descorme, and D. Duprez, "Towards the comprehension of oxygen storage processes on model three-way catalysts," Catalysis Today, vol. 73, no. 3-4, pp. 233-238, 2002.

[20] M. Boaro, M. Vicario, C. de Leitenburg, G. Dolcetti, and A. Trovarelli, "The use of temperature-programmed and dynamic/transient methods in catalysis: characterization of ceria-based, model three-way catalysts," Catalysis Today, vol. 77, no. 4, pp. 407-417, 2003.

[21] M. J. Rokosz, *et al.*, "Characterization of phosphorus-poisoned automotive exhaust catalysts," Applied Catalysis B: Environmental, vol. 33, no. 3, pp. 205-215, 2001.

[22] L. Xu, *et al.*, "Cerium phosphate in automotive exhaust catalyst poisoning," Applied Catalysis B: Environmental, vol. 50, no. 2, pp. 113-125, 2004.

[23] C. Larese, *et al.*, "Deactivation of real three-way catalysts by $CePO_4$ formation," Applied Catalysis B: Environmental, vol. 40, no. 4, pp. 305-317, 2003.

[24] D. Uy, A. E. O'Neill, L. Xu, W. H. Weber, and R. W. McCabe, "Observation of cerium phosphate in aged automotive catalysts using Raman spectroscopy," Applied Catalysis B: Environmental, vol. 41, no. 3, pp. 269-278, 2003.

[25] C. Xie, *et al.*, "Impact of lubricant additives on the physicochemical properties and activity of three-way catalysts," Catalysts, vol. 6, no. 4, p. 54, 2016.

[26] D. Kim, T. J. Toops, K. Nguyen, D. Brookshear, M. J. Lance, and J. Qu, "Impact of lubricant oil additives on the performance of Pd-based three-way catalysts," Emission Control Science Technology, vol. 6, pp. 139-150, 2020.

[27] D. Kim and J. Nam, "Impact of high-temperature desulfation on the performance of Pd-based TWC," Journal of Advanced Marine Engineering and Technology, vol. 45, no. 1, pp. 10-16, 2021.

[28] R. K. Herz, "Dynamic behavior of automotive catalysts. 1. Catalyst oxidation and reduction," Industrial & Engineering Chemistry Product Research and Development, vol. 20, no. 3, pp. 451-457, 1981.

[29] A. Trovarelli, "Catalytic properties of ceria and CeO_2-containing materials," Catalysis Reviews, vol. 38, no. 4, pp. 439-520, 1996.

[30] S. Bedrane, C. Descorme, and D. Duprez, "Investigation of the oxygen storage process on ceria- and ceria–zirconia-supported catalysts," Catalysis Today, vol. 75, no. 1-4, pp. 401-405, 2002.